Preparation and Electrochemical Performance of MnO$_2$/Fe$_3$O$_4$/MWCNTs nanocomposites as Anode for a Lithium-ion Battery

Huaixin Liu[*], *Xuemei Li, Guoqiang Xing*

College of Chemistry and Chemical Engineering, Shanxi Datong University, Datong 037009, Shanxi, China
[*]E-mail: Liuhuaixinji@163.com

This paper was conducted on preparation and electrochemical performance of MnO$_2$/Fe$_3$O$_4$/MWCNTs nanocomposites as a Lithium-ion Battery Anode Material. For this purpose, hydrothermal synthesized MnO$_2$ and Fe$_3$O$_4$ nanoparticles and carboxylated multi-walled carbon nanotubes (MWCNTs) were used for preparation of MnO$_2$/MWCNTs, Fe$_3$O$_4$/MWCNTs and MnO$_2$/Fe$_3$O$_4$/MWCNTs nanocomposites. The structural characterization and electrochemical properties of prepared nanocomposites were studied. Results exhibited the high porosity and high density of both types of nanoparticles were incorporated on MWCNTs and high aspect ratio of MWCNT-based nanocomposites were prepared. The cyclic voltammetry (CV) and electrochemical impedance spectroscopy (EIS) measurements showed that synergistic incorporation of MnO$_2$ and Fe$_3$O$_4$ nanoparticles in nanocomposite improves the dynamic behavior and facilitates the electron transport between the nanocomposite and the electrolyte. The discharge capacities MnO$_2$/Fe$_3$O$_4$/MWCNTs nanocomposite for initial and after 70th cycle was obtained of 207.1 and 189.5 mAh g^{-1} at 50 mA g^{-1}, respectively. Furthermore, the highest capacity retention was recorded of 93.3% and 91.0% for MnO$_2$/Fe$_3$O$_4$/MWCNTs at 50 mA g^{-1} and 700 mA g^{-1} after 70 cycles, respectively. Therefore, result showed that the MnO$_2$/Fe$_3$O$_4$/MWCNTs nanocomposite possesses more appropriate electrochemical properties than the MWCNTs, MnO$_2$/MWCNTs, and Fe$_3$O$_4$/MWCNTs nanocomposites because of the highest recorded values of discharge voltage plateau and specific capacity and more cycling stability and reversibility. The synergistic incorporation of MnO$_2$ and Fe$_3$O$_4$ nanoparticles in MWCNTs promoted the cycling and charge–discharge performances of composite.

1. INTRODUCTION

Nowadays development in technology of rechargeable batteries is a big challenge for all industries because of increasing societal demands for application of portable optoelectronic and electric

vehicles in medical science, military and mobile communications. Many studies are conducted on lead-acid [1], nickel-cadmium [2], nickel-metal hydride [3], lithium-ion polymer [4], and lithium-ion [5-7] as rechargeable batteries. There is considerable attention in lithium ion batteries because of its superior energy density over other rechargeable battery technologies, cost-effective, relatively low self-discharge, low maintenance and low toxicity [8-10]. However, these batteries need modification because of several disadvantages such as their aging negative effects, requirement to protect circuit, chemical changing of contents and heat generation in charging time [11-13]. Moreover, miniaturization of portable batteries is another factor for more applicable. Thus, development of lithium-ion battery industry depended on improving safety, capacity, cycle life, and charge–discharge rates properties using suitable nanostructured materials in both electrodes and electrolyte structures.

In order to modification the electrode the various nano-scale materials are studied such as Metal oxides, oxysalts, phosphates, carbonates, silicates, vanadium oxides , sulfides , carbon black, carbon nanotubes, molybdenum oxides and graphene [14-16]. Between these materials, carbon nanotubes (CNTs) are the most promising materials to improve lithium ion batteries because of their excellent electrochemical stability and good mechanical and electrical properties [17, 18]. Therefore, by considering the lower weight loading of CNTs and higher theoretical capacity (1000 mAh·g^{-1}) than other carbon structures such as graphite or black carbon, the interpolation of CNTs exhibits more effective strategy to promote the efficiency of Lithium-ion Batteries [19, 20].

Moreover, Fe_2O_3 is one of the appropriate candidates to fabrication of CNT composite-based anodes in lithium ion batteries due to its low cost, High-availability, eco-friendly and high theoretical capacity of 1005 mAh·g^{-1} [21]. It shows an excellent redox performance [22-24]. Furthermore, for improvement the electrochemical performance of the Fe_2O_3/CNTs composites-based anodes, the crystallinity, size, morphology and concentration of the materials are optimized [25]. For example, there are many electrochemical studies of SnO_2-Fe_2O_3@carbon [26], and NiO/Fe_3O_4/rGO [27] nanocomposites for developments in battery electrochemical activity. Manganese is an inexpensive and environment friendly transition metal that was utilized in batteries and gas sensors [28-31]. MnO_x have been also studied as the suitable candidate battery material because of high theoretical capacity (>700 mAh g^{-1}) [32]. Therefore, this study was carried out for electrochemical evaluation of the MnO_2/Fe_3O_4/MWCNTs nanocomposites as a lithium-ion battery anode material.

2. EXPERIMENTAL

The MnO_2 nanoparticles were synthesized using hydrothermal method accordance [33]. The mixture aqueous solutions of $KMnO_4$ (99.3%, Lianyungang, Jiangsu, China) and $MnSO_4$ (99%, Eisen-Golden Laboratories, USA) were prepared in a molar ratio of (1: 1). HNO_3 (98%, Jungar Banner Xinrong Chemicals Co., Ltd., China) was used to adjust the pH~1 of prepared solution and transferred in autoclave at 150°C for 24 hours. The reaction products were filtered (0.2 μm, Whatman polytetrafluoroethylene, Merck, Germany) and washed sequentially with deionized water and ethanol (99%, Briture Co., Ltd., China) for several times. The filtered nanoparticles were ultrasonically dispersed in 10 ml of ethanol.

In order to synthesis the Fe_3O_4 nanoparticles [34], the homogeneous green mixture of 30 ml of polyethylene glycol (PEG, molecular weight of 20000, Merck, Germany) and 5mM aqueous solution of $FeSO_4 \cdot 7H_2O$ (99%, Merck, Germany) was prepared and transferred in an autoclave at 100°C for 24 hours. The obtained suspension was rinsed by deionized water and ethanol for several times, respectively. Finally, the black synthesized Fe_3O_4 nanoparticles dispersed in 10 ml of ethanol.

In next step for carboxylation the MWCNTs, 1 g of commercial MWCNTs (95 wt %, 10–30 μm, Time Nano, China) were sonicated in a mixture of HNO_3/H_2SO_4 (98%, Wuhan Kangzheng Science and Technology Co., Ltd., China) in volume ratio of (1: 3) for 60 minutes. Then, the carboxylated MWCNTs were filtered (2 μm, Millipore nylon filter membrane, Merck, Germany) and washed by deionized water and dispersed in 10 ml of ethanol, respectively

In final step for synthesis of $MnO_2/Fe_3O_4/MWCNTs$ nanocomposites, the mixture of carboxylated carbon nanotubes and MnO_2 and Fe_3O_4 nanoparticles in volume ratio of (2: 1: 1) were sonicated for 20 minutes. For synthesis of $Fe_3O_4/MWCNTs$ and $MnO_2/MWCNTs$ nanocomposites, the mixture of carboxylated carbon nanotubes and nanoparticles was selected in volume ratio of (2: 1). Subsequently, the mixture was transferred on the magnetic stirring plate and heated at 65°C for 60 minutes. The final product was dried in room temperature and washed with deionized water.

Commercial lithium-ion battery electrolyte was prepared with a mixture of 1 M LiPF6 solution and ethylene carbonate-dimethyl carbonate-ethyl methyl carbonate (EC/DMC/EMC) with a volume ratio of (1:1:1). The working electrode were prepared of the mixture of synthesized nanocomposites, acetylene black and polyvinylidene fluoride (PVDF 5130, Shandong Gelon Lib Co.,Ltd., China) at ratio of (10:1:1) in 1-methyl-2-pyrrolidone (99%, Sigma-Aldrich, USA). Then, the prepared mixture was transferred to copper foils (1 cm^2) in the oven and dried at 70°C for 7 hours. The weight of the resulting mixture on copper foil was 1 mg which assembled in a coin-cell. Finally, the coin-cell 2032 as cathode, prepared electrodes as anode electrode, and Celgard 2325 as a separator were assembled in a glove box under the Argon atmosphere.

The morphology of synthesized nanocomposites was analyzed by scanning electron microscopy (SEM, Carl Zeiss SMT, Jena, Germany). The crystal structures of samples were analyzed with Xpert Pro X-ray diffractometer in wavelength of 1.5404 Å (Cu Kα) and 40KV/30 mA in power. The charge/discharge measurements of cells were conducted Neware battery measurement system (CT-3008, Neware technology, Shenzhen, China) with a range of 1.5–4.0 V. Cyclic voltammetry and EIS measurements were recorded on electrochemical potentiostat/galvanostat system (PGSTAT 30 Autolab, Eco Chemie, Switzerland). EIS tests were conducted on frequency range from 10^{-3} to 10^5 Hz at a potentiostatic signal amplitude of 5 mV.

3. RESULTS AND DISCUSSION

The SEM images of the MWCNTs and $MnO_2/Fe_3O_4/MWCNTs$ are presented in Figure 1. The SEM image of MWCNTs in Figure 1a shows the high aspect ratio of nanotubes in diameter of around 80 nm and average length less than 3 μm. $MnO_2/Fe_3O_4/MWCNTs$ SEM image in Figure 1b exhibits the high porosity and high density of both types of nanoparticles were incorporated on MWCNTs. It is

suggested utilizing MnO_2 nanoparticles in prepared composite can reduce aggregation phenomena in Fe_3O_4 nanoparticles and create the uniform distribution of resulting nanocomposite. Therefore, it can enhance the stability of the obtained functionalized nanoparticles on MWCNTs surface [35, 36].
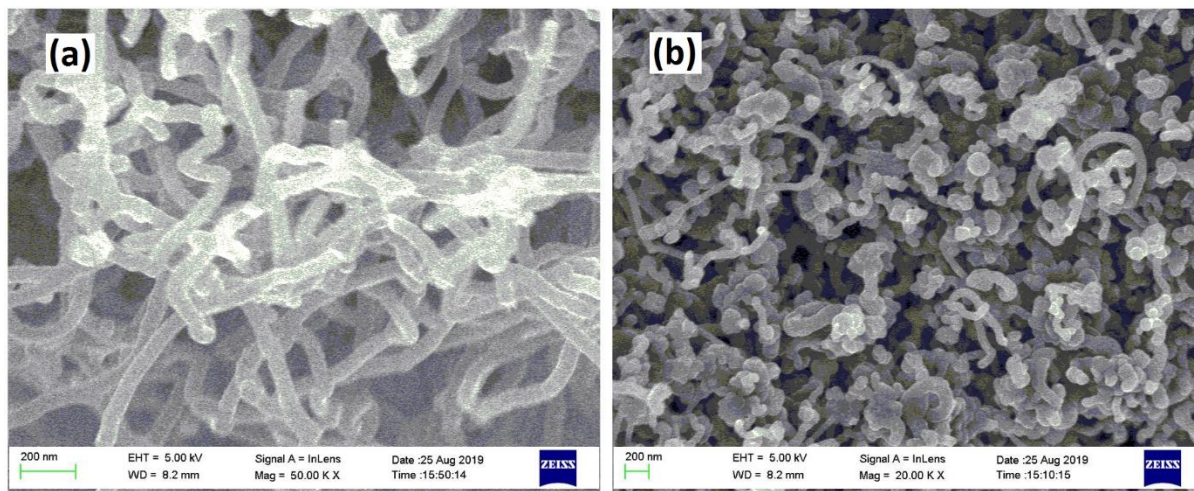
Figure 1. SEM images of (a) MWCNTs, (b) MnO_2/Fe_3O_4/MWCNTs nanocomposites

The XRD patterns of the MWCNTs, MnO_2/MWCNTs, Fe_3O_4/MWCNTs and MnO_2/Fe_3O_4/MWCNTs, are presented in Figure 2.
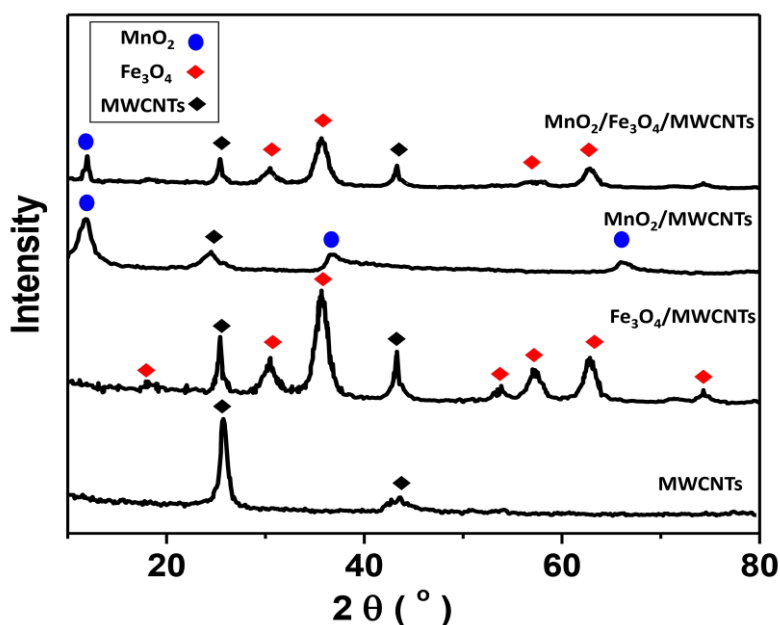
Figure 2. XRD patterns of MWCNTs, MnO_2/MWCNTs, Fe_3O_4/MWCNTs and MnO_2/Fe_3O_4/MWCNTs nanocomposites

The sharp diffraction peak is observed at $2\theta = 26.33°$ for XRD pattern of MWCNTs that it could display the high crystallinity and referred to (002) reflection of graphite crystal in MWCNTs structures [37]. This MWCNTs peak is observed in all XRD patterns of nanocomposites which indicates the successful preparation of MWCNTs nanocomposites. Another low intense peak in the XRD pattern of MWCNTs is observed at $2\theta = 44.38°$ that it reflects the (100) plane of the MWCNTs. The XRD pattern of Fe_3O_4/MWCNTs shows peaks at $2\theta = 18.10°, 30.11°, 35.51°, 53.02°, 57.10°, 62.53°$, and $74.54°$ which assigning to the (111) (220), (311), (422), (511), (440), and (533) planes of synthesized Fe_3O_4 nanoparticles in the cubic spinel crystal structure (JCPDS Card. No. 79-0418). In XRD pattern of MnO_2/MWCNTs nanocomposite, diffraction peaks of birnessite-type MnO_2 phase is observed because of diffraction peak at $2\theta = 12.11°, 37.15°$ and $66.25°$ which reflect to (001), (111) and (312) planes (JCPDS Card. No. 80-1098). Moreover, the XRD pattern of MnO_2/Fe_3O_4/MWCNTs shows the peaks of MnO_2, Fe_3O_4 and MWCNTs that indicate that the nanocomposite has been prepared of a mixture of three nanostructures in this method.

Figure 3a shows the initial discharge and charge profiles of the prepared nanocomposites at a current density of 50 mA g^{-1} in the voltage range of 1.5 – 4.0 V. As seen, the initial discharge capacities of MWCNTs, MnO_2/MWCNTs, Fe_3O_4/MWCNTs and MnO_2/Fe_3O_4/MWCNTs nanocomposites are recorded of 189.9, 200.1, 210.2 and 207.1 mAh g^{-1}, respectively. Moreover, Figure 3b shows that the discharge capacities of the MWCNTs, MnO_2/MWCNTs, Fe_3O_4/MWCNTs and MnO_2/Fe_3O_4/MWCNTs nanocomposites were recorded 162.2, 170.3, 179.9 and 189.5 mAh g^{-1} after 70 cycles, respectively. Result exhibits that the MnO_2/Fe_3O_4/MWCNTs nanocomposite possesses appropriate electrochemical properties than the other prepared MWCNTs based nanocomposites because of the highest recorded values of discharge voltage plateau and specific capacity. Therefore, this nanocomposite can exhibit the low electrochemical polarization because of the lithium transport efficiency for Li-ion batteries [38-40].
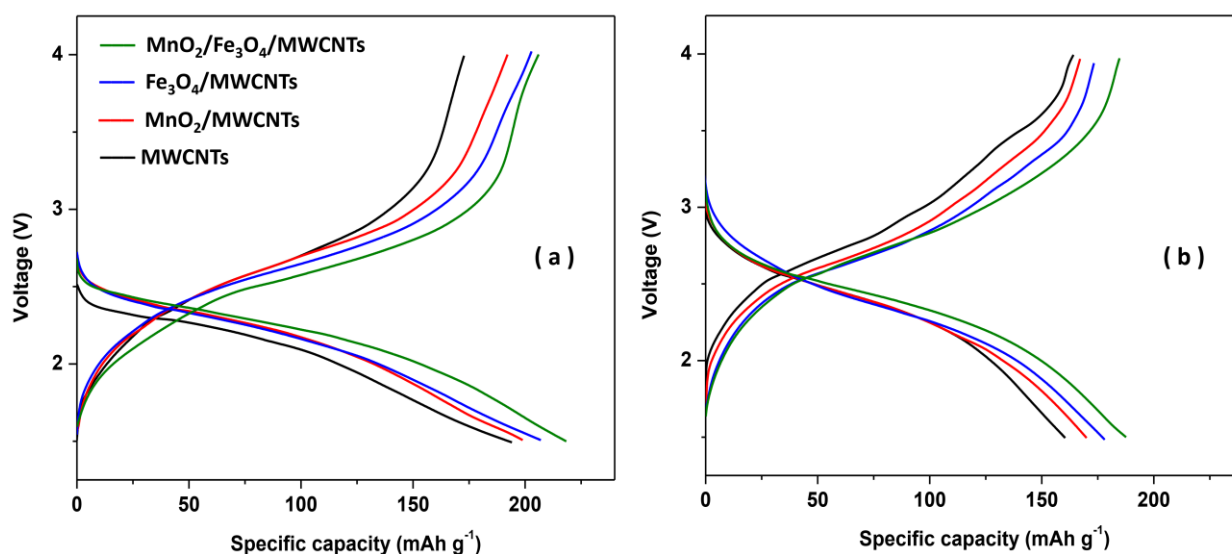
Figure 3. (a) First cycle and (b) the 70th cycle charge/discharge profiles of MWCNTs, MnO_2/MWCNTs, Fe_3O_4/MWCNTs and MnO_2/Fe_3O_4/MWCNTs nanocomposite electrodes at a current density of 50 mA g^{-1} in the voltage range of 1.5-4.0 V.

In order to study the cycling performances of the prepared MWCNTs based nanocomposites, the cycling performances of MWCNTs, MnO_2/MWCNTs, Fe_3O_4/MWCNTs and MnO_2/Fe_3O_4/MWCNTs nanocomposites at 50 mA g^{-1} and 700 mA g^{-1} in the voltage range of 1.5 – 4.0 V over 70 cycles were recorded in Figure 4. As shown, the Coulombic efficiencies of prepared nanocomposites are more than 96.5%. Moreover, capacity retention of the prepared electrodes at 50 mA g^{-1} and 700 mA g^{-1} in voltage profile are presented in Table 1. It is observed that the highest capacity retention rates are recorded of 93.3% and 91.0% for MnO_2/Fe_3O_4/MWCNTs at 50 mA g^{-1} and 700 mA g^{-1}, respectively. Therefore, the cycling stability of MnO_2/Fe_3O_4/MWCNTs is considerably better than other prepared electrodes.
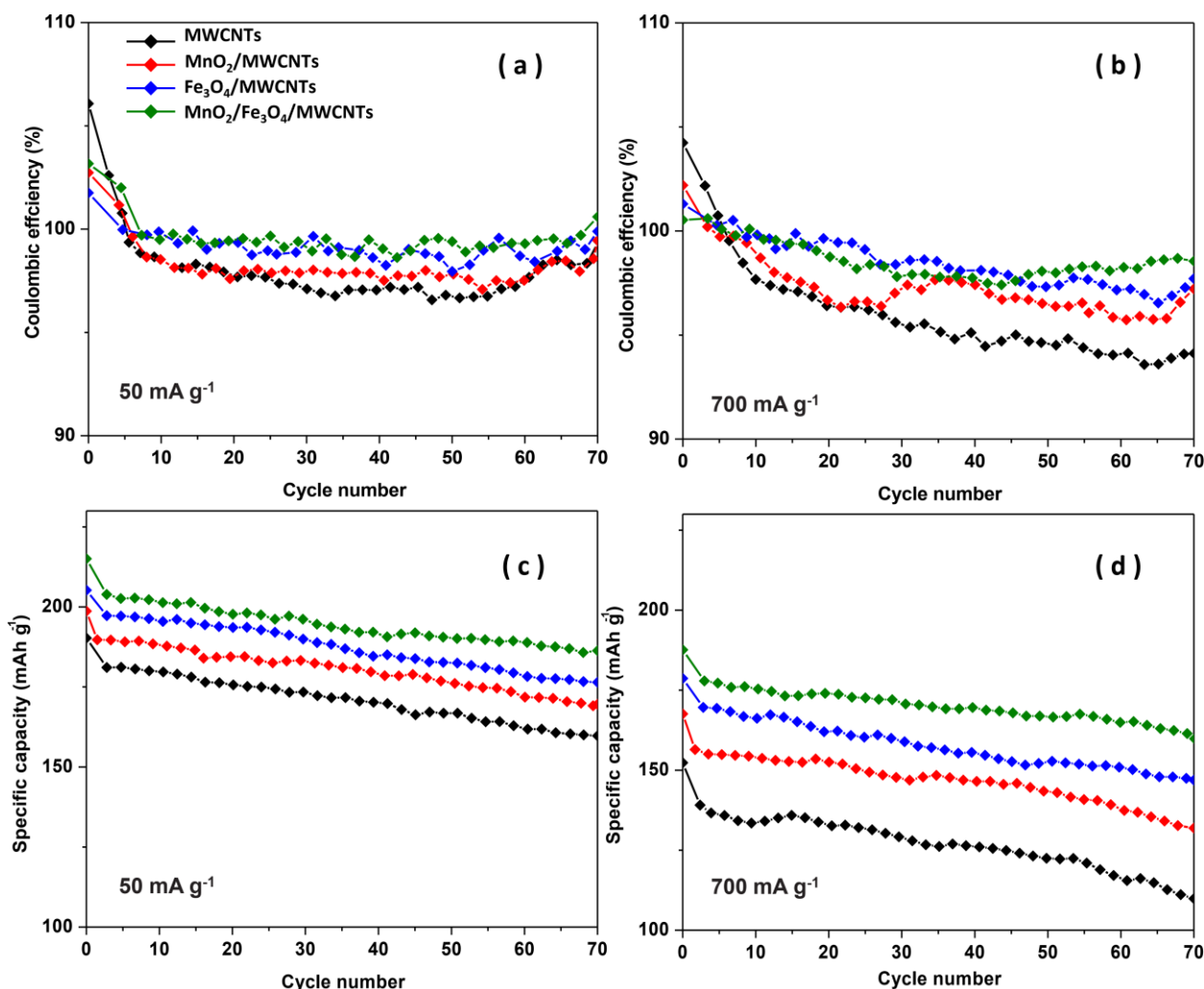
Figure 4. Cycling performances of MWCNTs, MnO_2/MWCNTs, Fe_3O_4/MWCNTs and MnO_2/Fe_3O_4/MWCNTs nanocomposite electrodes at current densities of 50 mA g^{-1} C and 700 mA g^{-1}.

In order to further study of electrochemical performances of the MWCNTs, MnO_2/MWCNTs, Fe_3O_4/MWCNTs and MnO_2/Fe_3O_4/MWCNTs nanocomposites were recorded at a scan rate of 0.1 mV s^{-1} in Figure 5. As observed, there are the similar pairs of reversible redox peaks which assign to the similar electrochemical response of electrodes in insertion/extraction of Li^+. As shown, the ΔE values (the difference between the anodic and cathodic peak) of MWCNTs, MnO_2/MWCNTs, Fe_3O_4/MWCNTs

and $MnO_2/Fe_3O_4/MWCNTs$ nanocomposites are about 0.29, 0.34, 0.31 and 0.25 V, respectively. This exhibits that the highest polarization is belonging to the $MnO_2/MWCNTs$ nanocomposite. Furthermore, minimum value of ΔE and maximum values of current and area of the recorded CV take place for $MnO_2/Fe_3O_4/MWCNTs$ nanocomposite that these quantities are correlated to the obtained capacity [41]. Consequently, incorporation of MnO_2 and Fe_3O_4 nanoparticles in MWCNTs can promote the cycling and charge–discharge performances of composite.

Table 1. Result of cycling performances

Nanocomposite	Capacity retention (%)	
	50 mA g^{-1}	700 mA g^{-1}
MWCNTs	87.6	77.1
$MnO_2/MWCNTs$	90.1	85.1
$Fe_3O_4/MWCNTs$	89.2	83.4
$MnO_2/Fe_3O_4/MWCNTs$	93.3	91.0
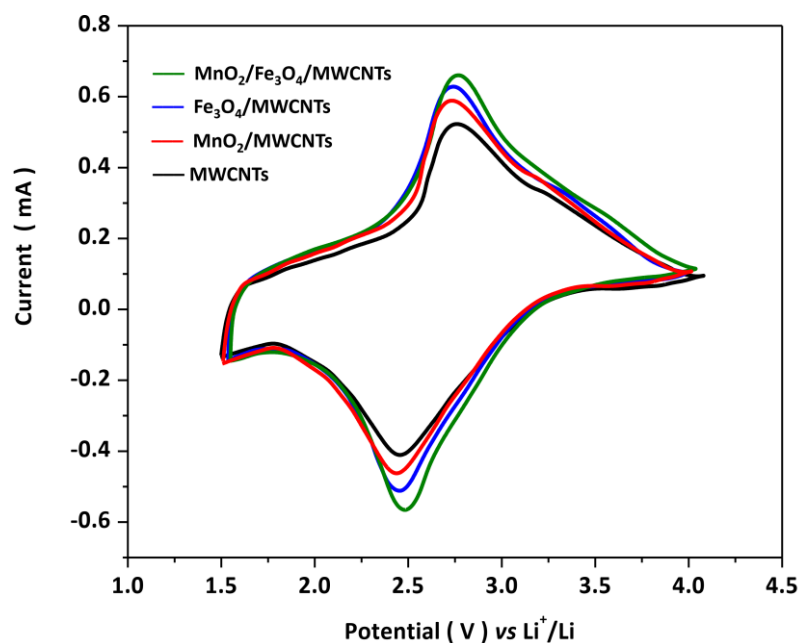
Figure 5. The recorded CVs of MWCNTs, $MnO_2/MWCNTs$, $Fe_3O_4/MWCNTs$ and $MnO_2/Fe_3O_4/MWCNTs$ nanocomposites at 50 mA g^{-1} in the voltage range of 1.5–4.0 V at scan rate of 0.1 mV s^{-1}.

To evaluate the rate performance of the prepared nanocomposites, the rate performance plots were recorded at current densities of 20, 100, 500, 1000 and 2000 mA g^{-1} in Figure 6. As observed for all samples, with increasing the current density, the discharge capacity is decreased. The capacity retentions of MWCNTs, $MnO_2/MWCNTs$, $Fe_3O_4/MWCNTs$ and $MnO_2/Fe_3O_4/MWCNTs$ nanocomposites are 73.1, 91.1, 93.1 and 93.8%, respectively. In order to study the stability and reversibility, rate performance of samples were again recorded at 20 mA g^{-1}. Additionally,

$MnO_2/Fe_3O_4/MWCNTs$ nanocomposite shows significant improvement in capacity retention, rate capability, stability and reversibility.
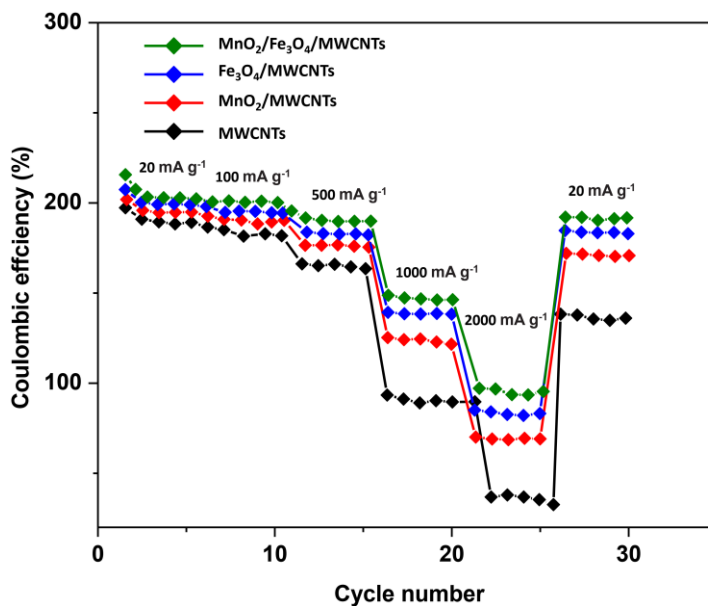
Figure 6. Discharge capacities of MWCNTs, $MnO_2/MWCNTs$, $Fe_3O_4/MWCNTs$, and $MnO_2/Fe_3O_4/MWCNTs$ nanocomposites at various current densities from 20 to 2000 mA g^{-1}.
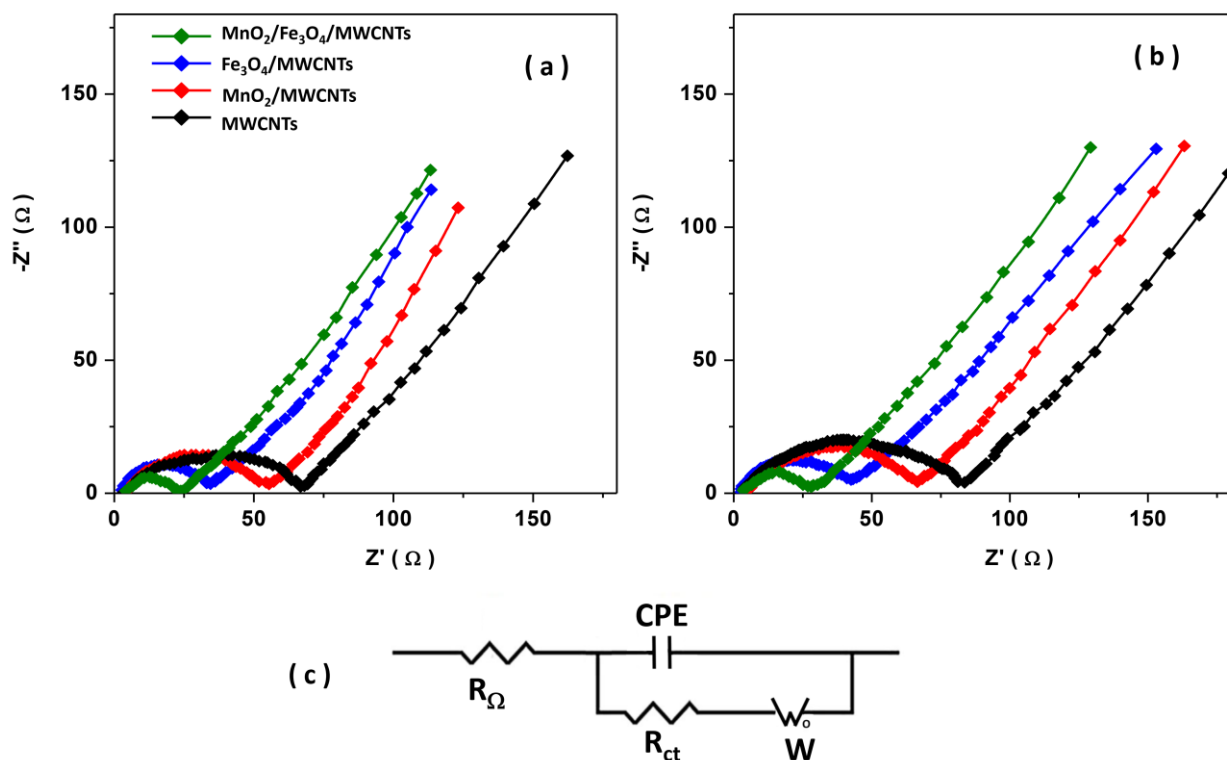
Figure7. The impedance plots of (a) the first and (b) 70th cycles of MWCNTs, $MnO_2/MWCNTs$ $Fe_3O_4/MWCNTs$ and $MnO_2/Fe_3O_4/MWCNTs$ nanocomposites; (c) the equivalent circuit model.

Figure 7 exhibits the EIS plots and the equivalent circuit model of MWCNTs, MnO_2/MWCNTs, Fe_3O_4/MWCNTs and MnO_2/Fe_3O_4/MWCNTs nanocomposites in first and after the 70th cycles at room temperature. As seen, the Nyquist plots with a semicircle at high frequency ($10^3 – 10^5$ Hz) and a linear tail at low frequency ($10^{-3} – 10^3$ Hz). The semicircle is associated with the diffusion and transfer process of Li^+ through the solid electrolyte interface on the active sites of nanoparticles [27]. The slope of linear tail in low frequency region is attributed to Warburg impedance (W) which shows the solid-state diffusion of Li^+ in active materials [27, 42, 43]. The equivalent circuit of the nanocomposites is presented in Figure 7c where R_Ω, R_{ct} are the electrolyte resistance and the Li^+ charge transfer resistance at the interface. CPE is the capacity of double-layer and the passivation film. The plots obviously demonstrate that the conductivity of MnO_2/Fe_3O_4/MWCNTs nanocomposite and its electron transfer efficiency are enhanced which due to decreasing the charge transfer resistance at the electrode interface. It illustrates that coexistence of MnO_2 and Fe_3O_4 nanoparticles in nanocomposite facilitates the electron transport between the nanocomposite and the electrolyte which depends on the frequency of ion diffusion/transfer to the electrode surface [44]. Therefore, MnO_2/Fe_3O_4/MWCNTs nanocomposite shows excellent electrochemical properties as an anode material for Lithium-ion batteries. It should be considered homogeneous MnO_2 and Fe_3O_4 nanoparticles are incorporated on the surface of the MWCNTs and generate the large surface area on the electrode surface. In consequence, the large electrode/ electrolyte interface are formed and leads to decrease the diffusion paths of the Li^+ ions [45, 46]. Nano-scale of MnO_2, Fe_3O_4 and CNTs leads to decrease the potential barrier to electron transfer and increase the electron transmission rate which is an important factor to improve the both specific capacitance and rate capability values. In addition, MWCNTs enhance the electrical conductivity of the modified electrode [47]. The dispersion of MnO_2 nanoparticles in MWCNTs textures and between the Fe_3O_4 nanoparticles prevents aggregation of the magnetic Fe_3O_4 structures which is useful for cycling stability [44, 48].

Moreover, the comparison of performance of MWCNTs, MnO_2/MWCNTs, Fe_3O_4/MWCNTs and MnO_2/Fe_3O_4/MWCNTs nanocomposites with the other reported CNTs and Fe-based composites as anode material for lithium-ion batteries is presented in Table 2. As shown, there are higher value of first cycle discharge for reported CNTs and Fe-based composites [29, 49-54] but the higher Coulombic efficiency is obtained for MnO_2/Fe_3O_4/MWCNTs nanocomposite which indicates a long battery cycle life [55].

Table 2. Performance comparisons of MWCNTs, MnO$_2$/MWCNTs, Fe$_3$O$_4$/MWCNTs and MnO$_2$/Fe$_3$O$_4$/MWCNTs nanocomposites with the other reported CNTs and Fe-based composites as anode material for Lithium-ion batteries

Anode materials	First cycle discharge (mAh g^{-1})	Coulombic efficiency (%)	Current density (mA g^{-1})	Ref
MWCNTs	189.9	96	50	This work
MnO$_2$/MWCNTs	200.1	97	50	This work
Fe$_3$O$_4$/MWCNTs	210.2	97	50	This work
MnO$_2$/Fe$_3$O$_4$/MWCNTs	207.1	98	50	This work
N-doped graphene/Fe–Fe$_3$C	904	24	100	[29]
CoO/N-CNTs	1250	83	100	[49]
Cage-like CNTs/Si	730	68	100	[50]
CNT/N- Si	-	80	-	[51]
CuO/CNT	-	56	100	[52]
Fe$_3$O$_4$/C/CNTs	-	75.7	200	[53]
Porous Fe3O4/C	1796	56.2	100	[54]

4. CONCLUSION

In this study, MnO$_2$ and Fe$_3$O$_4$ nanoparticles were synthesized using hydrothermal method and mixed with carboxylated carbon nanotubes for preparation of MnO$_2$/MWCNTs, Fe$_3$O$_4$/MWCNTs and MnO$_2$/Fe$_3$O$_4$/MWCNTs nanocomposites. The morphology and structure characterization of prepared nanocomposites were carried out using SEM and XRD analyses. The electrochemical properties were conducted with charge/discharge, EIS and CV analyses. Results of SEM and XRD analyses displayed the high porosity and high density of both types of nanoparticles were homogeneously mixed with MWCNTs. The CV and EIS measurements illustrate that coexistence of MnO$_2$ and Fe$_3$O$_4$ nanoparticles in nanocomposite ameliorates the dynamic behavior of nanocomposite and simplifies the electron transport between the electrode and the electrolyte. The highest capacity retention was obtained 93.3% and 91.0% for MnO$_2$/Fe$_3$O$_4$/MWCNTs at 50 mA g^{-1} and 700 mA g^{-1} after 70 cycles, respectively. Therefore, it is concluded that the MnO$_2$/Fe$_3$O$_4$/MWCNTs nanocomposite showed better electrochemical properties than the MWCNTs, MnO$_2$/MWCNTs, and Fe$_3$O$_4$/MWCNTs nanocomposites due to the highest recorded values of discharge voltage plateau and specific capacity and high cycling stability and reversibility. The synergistic incorporation of MnO$_2$ and Fe$_3$O$_4$ nanoparticles in MWCNTs enhanced the cycling and charge–discharge activities of nanocomposite.

References

1. P. Kurzweil, *Journal of Power Sources*, 195 (2010) 4424.
2. C. Jeyaseelan, A. Jain, P. Khurana, D. Kumar and S. Thatai, *Rechargeable Batteries: History, Progress, and Applications*, (2020) 177.
3. U. Morali and S. Erol, *Journal of the Faculty of Engineering and Architecture of Gazi University*, 35 (2020) 297.
4. A.R. Polu and H.-W. Rhee, *International Journal of Hydrogen Energy*, 42 (2017) 7212.
5. M. Imperiyka, A. Ahmad, S. Hanifah and M. Rahman, *International Journal of Electrochemical Science*, 8 (2013) 10932.
6. X. Huang, J. Wu, Y. Lin and R. Guo, *International Journal of Electrochemical Science*, 7 (2012) 6611.
7. H. Karimi-Maleh and O.A. Arotiba, *Journal of colloid and interface science*, 560 (2020) 208.
8. P. Wu, G. Shao, C. Guo, Y. Lu, X. Dong, Y. Zhong and A. Liu, *Journal of Alloys and Compounds*, 802 (2019) 620.
9. A. Khodadadi, E. Faghih-Mirzaei, H. Karimi-Maleh, A. Abbaspourrad, S. Agarwal and V.K. Gupta, *Sensors and actuators b: chemical*, 284 (2019) 568.
10. J. Rouhi, S. Mahmud, N. Naderi, C.R. Ooi and M.R. Mahmood, *Nanoscale research letters*, 8 (2013) 1.
11. T. Waldmann, A. Iturrondobeitia, M. Kasper, N. Ghanbari, F. Aguesse, E. Bekaert, L. Daniel, S. Genies, I.J. Gordon and M.W. Löble, *Journal of The Electrochemical Society*, 163 (2016) A2149.
12. A. Nazari and S. Farhad, *Applied Thermal Engineering*, 125 (2017) 1501.
13. H. Karimi-Maleh, F. Karimi, M. Alizadeh and A.L. Sanati, *The Chemical Record*, 20 (2020) 682.
14. J. Balach, J. Linnemann, T. Jaumann and L. Giebeler, *Journal of Materials Chemistry A*, 6 (2018) 23127.
15. Y. Zhao, L.P. Wang, M.T. Sougrati, Z. Feng, Y. Leconte, A. Fisher, M. Srinivasan and Z. Xu, *Advanced Energy Materials*, 7 (2017) 1601424.
16. M. Miraki, H. Karimi-Maleh, M.A. Taher, S. Cheraghi, F. Karimi, S. Agarwal and V.K. Gupta, *Journal of Molecular Liquids*, 278 (2019) 672.
17. S. Jessl, D. Beesley, S. Engelke, C. Valentine, J. Stallard, N. Fleck, S. Ahmad, M. Cole and M. De Volder, *Materials Science and Engineering: A*, 735 (2018) 1.
18. L. Nan, C. Yalan, L. Jixiang, O. Dujuan, D. Wenhui, J. Rouhi and M. Mustapha, *RSC Advances*, 10 (2020) 27923.
19. B.J. Landi, M.J. Ganter, C.D. Cress, R.A. DiLeo and R.P. Raffaelle, *Energy & Environmental Science*, 2 (2009) 638.
20. H. Karimi-Maleh, K. Cellat, K. Arıkan, A. Savk, F. Karimi and F. Şen, *Materials Chemistry and Physics*, 250 (2020) 123042.
21. T.R. Penki, S. Shivakumara, M. Minakshi and N. Munichandraiah, *Electrochimica Acta*, 167 (2015) 330.
22. H. Li, L. Jia, J.-l. Liang, H.-y. Yan, Z.-y. Cai and R.G. Reddy, *International Journal of Electrochemical Science*, 14 (2019)
23. A.A. Ismail, A.M. Ali, F.A. Harraz, M. Faisal, H. Shoukry and A. Al-Salami, *International Journal of Electrochemical Science*, 14 (2019) 15.
24. J. Rouhi, S. Kakooei, S.M. Sadeghzadeh, O. Rouhi and R. Karimzadeh, *Journal of Solid State Electrochemistry*, 24 (2020) 1599.
25. G. Gao, Y. Jin, Q. Zeng, D. Wang and C. Shen, *Beilstein Journal of Nanotechnology*, 8 (2017) 649.
26. J. Deng, Y. Dai, Z. Xiao, S. Song, H. Dai, L. Li and J. Li, *Nanomaterials*, 10 (2020) 249.
27. M. Pei, Y. Wu, Z. Qi and D. Mei, *Ionics*, (2020) 1.

28. X. Li, J. Liu, Y. Zhang, Y. Li, H. Liu, X. Meng, J. Yang, D. Geng, D. Wang and R. Li, *Journal of Power Sources*, 197 (2012)
29. Y. Tan, K. Zhu, D. Li, F. Bai, Y. Wei and P. Zhang, *Chemical Engineering Journal*, 258 (2014) 93.
30. X.-l. Huang, X. Zhao, Z.-l. Wang, L.-m. Wang and X.-b. Zhang, *Journal of Materials Chemistry*, 22 (2012) 3764.
31. J. Rouhi, M.R. Mahmood, S. Mahmud and R. Dalvand, *Journal of Solid State Electrochemistry*, 18 (2014) 1695.
32. C.-G. Han, C. Zhu, Y. Aoki, H. Habazaki and T. Akiyama, *Green Energy & Environment*, 2 (2017) 377.
33. T. Xiao, E. Strutt, M. Benaissa, H. Chen and B. Kear, *Nanostructured Materials*, 10 (1998) 1051.
34. S. Ni, X. Wang, G. Zhou, F. Yang, J. Wang, Q. Wang and D. He, *Materials Letters*, 63 (2009) 2701.
35. R.C. Popescu, E. Andronescu and B.S. Vasile, *Nanomaterials*, 9 (2019) 1791.
36. M. Alimanesh, J. Rouhi and Z. Hassan, *Ceramics International*, 42 (2016) 5136.
37. F.M. Anjalin, *Der. Pharma. Chemica*, 6 (2014) 354.
38. Y. Bai, X. Zhou, Z. Jia, C. Wu, L. Yang, M. Chen, H. Zhao, F. Wu and G. Liu, *Nano Energy*, 17 (2015) 140.
39. W. Wu, Y. Wang, X. Wang, Q. Chen, X. Wang, S. Yang, X. Liu, J. Guo and Z. Yang, *Journal of alloys and compounds*, 486 (2009) 93.
40. J. Rouhi, S. Mahmud, S. Hutagalung and S. Kakooei, *Micro & Nano Letters*, 7 (2012) 325.
41. T. Kim, W. Choi, H.-C. Shin, J.-Y. Choi, J.M. Kim, M.-S. Park and W.-S. Yoon, *Journal of Electrochemical Science and Technology*, 11 (2020) 14.
42. J. Rouhi, C.R. Ooi, S. Mahmud and M.R. Mahmood, *Electronic Materials Letters*, 11 (2015) 957.
43. R. Dalvand, S. Mahmud, J. Rouhi and C.R. Ooi, *Materials Letters*, 146 (2015) 65.
44. J. Jiao, W. Qiu, J. Tang, L. Chen and L. Jing, *Nano Research*, 9 (2016) 1256.
45. D. Liu, Q. Zhang, P. Xiao, B.B. Garcia, Q. Guo, R. Champion and G. Cao, *Chemistry of Materials*, 20 (2008) 1376.
46. Q. Wang, L. Jiao, H. Du, Y. Wang and H. Yuan, *Journal of Power Sources*, 245 (2014) 101.
47. Y. Li, H. Zhang, Z. Xiao and R. Wang, *Frontiers in chemistry*, 7 (2019) 555.
48. R. Dalvand, S. Mahmud and J. Rouhi, *Materials Letters*, 160 (2015) 444.
49. I. Khan, F. Nasim, M. Choucair, S. Ullah, A. Badshah and M. Nadeem, *RSC advances*, 6 (2016) 1129.
50. J. Shu, H. Li, R. Yang, Y. Shi and X. Huang, *Electrochemistry Communications*, 8 (2006) 51.
51. Z. Wen, K. Wang, L. Chen and J. Xie, *Electrochemistry Communications*, 8 (2006) 1349.
52. S. Ko, J.I. Lee, H.S. Yang, S. Park and U. Jeong, *Advanced materials*, 24 (2012) 4451.
53. J. Xiong, Y. Yang, J. Zeng, J. Wang and J. Zhao, *Journal of Materials Science*, 53 (2018) 16447.
54. W. Han, X. Qin, J. Wu, Q. Li, M. Liu, Y. Xia, H. Du, B. Li and F. Kang, *Nano Research*, 11 (2018) 892.
55. F. Yang, D. Wang, Y. Zhao, K.-L. Tsui and S.J. Bae, *Energy*, 145 (2018) 486.